Supplementary Information for:

Large loss of CO_2 in winter observed across the northern permafrost region

Authors: Susan. M. Natali*†, Jennifer D. Watts†, Brendan M. Rogers, Stefano Potter, Sarah M. Ludwig, Anne-Katrin Selbmann, Patrick F. Sullivan, Benjamin W. Abbott, Kyle A. Arndt, Leah Birch, Mats P. Björkman, A. Anthony Bloom, Gerardo Celis, Torben R. Christensen, Casper T. Christiansen, Roisin Commane, Elisabeth J. Cooper, Patrick Crill, Claudia Czimczik, Sergey Davydov, Jinyang Du, Jocelyn E. Egan, Bo Elberling, Eugenie S. Euskirchen, Thomas Friborg, Hélène Genet, Mathias Göckede, Jordan P. Goodrich, Paul Grogan, Manuel Helbig, Elchin E. Jafarov, Julie D. Jastrow, Aram A. M. Kalhori, Yongwon Kim, John Kimball, Lars Kutzbach, Mark J. Lara, Klaus S. Larsen, Bang-Yong Lee, Zhihua Liu, Michael M. Loranty, Magnus Lund, Massimo Lupascu, Nima Madani, Avni Malhotra, Roser Matamala, Jack McFarland, A. David McGuire, Anders Michelsen, Christina Minions, Walter C. Oechel, David Olefeldt, Frans-Jan W. Parmentier, Norbert Pirk, Ben Poulter, William Quinton, Fereidoun Rezanezhad, David Risk, Torsten Sachs, Kevin Schaefer, Niels M. Schmidt, Edward A.G. Schuur, Philipp R. Semenchuk, Gaius Shaver, Oliver Sonnentag, Gregory Starr, Claire C. Treat, Mark P. Waldrop, Yihui Wang, Jeffrey Welker, Christian Wille, Xiaofeng Xu, Zhen Zhang, Qianlai Zhuang, Donatella Zona

*Correspondence to: snatali@whrc.org
†Authors contributed equally to this work.

Supplementary Methods

Extracted *in situ* data

We compiled a dataset of *in situ* winter CO_2 emissions and potential driving variables from sites within the northern permafrost zone. To identify published flux data, we conducted a literature search using Web of Science and we also solicited unpublished data through the Permafrost Carbon Network, and other research networks. Unpublished data were processed and filtered by the data providers. Data were extracted directly from manuscript text and tables and from figures using Plot Digitizer (http://plotdigitizer.sourceforge.net/).

In addition to extracting winter CO_2 fluxes from the literature, we extracted relevant ancillary *in situ* data (*e.g.*, soil temperature, moisture, soil carbon). We extracted both percent soil carbon (C) and organic matter (SOM) when available and converted SOM to C assuming a conversion factor of 1.9[1]. Data were aggregated monthly or seasonally when monthly data were not available.

We included data collected using several measurement methods: 1. *Chamber:* chamber placed over the ground after digging a snow pit or placed underneath the snowpack prior to snow accumulation, and gas flux measured as a change in gas concentration in the chamber over time (measured at 35% of the locations in this synthesis); 2. *Chamber-snow:* chamber placed on top of the snow pack, and flux measured as a change in gas concentration in the chamber over time (measured at 3% of locations); 3. *Diffusion:* Gas concentrations measured at two or more locations through the snow pack, and gas flux calculated based on gas diffusion rate through the snowpack (measured at 30% of locations); 4. *Eddy covariance*: Gas flux calculated based on covariance of gas concentration and vertical wind velocity; separated into closed path (air is drawn in through a sampling tube to an infrared gas analyzer; measured at 12% of locations) and open path (air passes freely between infrared source and detector; measured at 9% of locations) systems; 5. *Soda lime*: Seasonal release of CO_2 from soils determined from CO_2 adsorption onto soda lime placed in a closed chamber on top of the soil (measured at 11% of locations). Examples of each of these methods can be found within the references cited in Supplemental Information (SI) Table 1; soil temperature and flux distribution by measurement method is shown in SI Figure 6; and comparisons of methods, including limitations can be found in[2-4]. We used the full dataset including all measurement methods for upscaling and future projections, because excluding data from the machine-learning model based on collection method did not substantially change assessments of model uncertainty.

We did not distinguish between heterotrophic and autotrophic sources of winter CO_2 emissions; however, we expect that winter emissions are primarily microbially derived. While contributions of root respiration to winter CO_2 efflux are expected to be negligible[5], this is a major unknown, and common methods for partitioning soil respiration (e.g., trenching/girdling, carbon isotopes) are often unable to distinguish between microbial and plant respiration of recently-fixed photosynthates.

Data extraction, geospatial data

Historical climatological data (mean annual, seasonal and monthly air temperature and precipitation) were obtained from the WorldClim database (1960–1990; 1 km^2 resolution)[6]. Monthly aggregated air and soil temperature during the measurement intervals were obtained from NASA Modern-Era Retrospective Analysis for Research Applications, Version 2 (MERRA-2; 1/2 x 2/3° resolution; 2003-2017) product[7]. Mean volumetric soil moisture (VSM) of the litter/soil surface for the measurement month (or, if frozen, for the last unfrozen month) and June-July months prior to the flux measurement were calculated using the University of Montana Advanced Microwave Scanning Radiometer (AMSR) Land Parameter Data Record (LPDR; 25 km; 2003-2017)[8]. Mean soil wetness fraction of the root zone during the measurement month and previous July-August were provided by the MERRA-2 land model component (2003-2017)[9]. Mean monthly snow water equivalent (SWE) for the measurement month was obtained from the European Space Agency's GlobSnow Version 2 monthly aggregated SWE product (L3B SWE; 25 km resolution; 1979-2016). We used GlobSnow because it is well documented, has a strong research user base, and because gridded error estimates are provided along with the snow cover and SWE retrievals. Although depth and density are key parameters influencing winter CO_2 fluxes through their impact on soil thermal regimes[10,11], *in situ* snow data had low coverage in the synthesis dataset and the spatiotemporal resolution of SWE and other available snow data products were unable to capture snow-temperature-CO_2 flux dynamics for our study domain and, therefore, were not retained in the final analysis of this study.

Soil carbon stocks to 30 cm were obtained from the Northern Circumpolar Soil Carbon Database (NCSCD; 0.0012 degrees resolution)[12]; soil texture (% sand, silt, clay), bulk density, soil carbon density, and pH were extracted from the SoilGrids product (250 m)[13]. Permafrost condition was obtained from permafrost zone[14] and permafrost zonation index maps (1 km)[15]. Permafrost zones include continuous permafrost, which has permafrost underlying 90-100% of the landscape, discontinuous (50-90%), sporadic (10-50%) and isolated (0-10%) permafrost.

Land cover classifications were derived from the Circumpolar Arctic Vegetation Map (CAVM; 1:7.5M scale)[16] for tundra sites and the European Space Agency (ESA) Climate

Change Initiative (CCI) V.2 land cover classifications (300 m)[17] for boreal sites (SI Figure 5, SI Table 4). We extracted enhanced vegetation index (EVI) from the MODIS MOD13Q1 product (2001-2016, 16 day sampling, 250 m resolution)[18] and calculated average and maximum EVI for the prior growing season (~ June 9 - August 28) and for the 2001-2016 interval for each site. We used MODIS MOD44B V6 for tree cover[19] during the measurement year (or yr. 2000 for earlier data) and MODIS MOD15 Collection 6[20] for maximum leaf area index (LAI) in the summer prior to winter flux measurements. All MODIS data were quality screened to include only those data having a pixel level quality assurance bit code of 00 indicating "data produced - good quality". We obtained cumulative annual and peak-summer (July, August) GPP for the summer prior to the flux measurements from the NASA Soil Moisture Active Passive (SMAP) Level 4 Carbon Version 3 product (9 km)[21] and from the MODIS MOD17 V0006 product (1 km)[22]. Fractional grid cell lake cover was obtained from the MOD44W MODIS/Terra land water mask (250 m)[23].

All geospatial data were re-gridded to the National Snow and Ice Data Center Equal Area Scalable Earth (EASE) 2.0 format[24] at a 25 km spatial resolution prior to the CO_2 flux upscaling and simulations.

Data filtering

We excluded modeled CO_2 flux data from the synthesis dataset, but included gap-filled data when the gap-filling model was based on data collected during the winter. We also excluded data that were averaged across multiple years. For eddy covariance data, we used fluxes of net ecosystem exchange (NEE) or, when fluxes were partitioned, ecosystem respiration, which were essentially the same during the winter. When a monthly winter flux was negative (*i.e.*, signifying

CO_2 uptake), we excluded that month from the analysis. Negative winter fluxes can occur under low CO_2 flux conditions and/or due to instrument-related error, particularly with open-path eddy covariance systems[25].

We filtered out monthly average CO_2 fluxes that were anomalously high (> 2 g C m^{-2} day^{-1}; n=4, 0.4% of data) and negative/zero fluxes (< 0.001 g C m^{-2} day^{-1}; n=5). To minimize the contribution from autotrophic CO_2 exchange, when the measurement method included aboveground vegetation (*e.g.*, eddy covariance; n=4), we filtered fluxes measured when *in situ* air temperatures were greater than 5° C and soil temperatures (0-25 cm) were greater than -1° C; we retained data with > 5° C air temperatures and > -1° C soil temperature when fluxes were measured below the snowpack. We excluded all data with reported soil temperatures greater than 2° C. Data were also filtered to reduce model overfitting resulting from limited data.

Calculation of Q10

The temperature response functions of *in situ* winter CO_2 fluxes and of CO_2 emissions from low temperature incubations were modeled with an exponential temperature response function (Eq. 1) using a Bayesian statistical approach.

Eq. 1: $flux = A*exp(B*Tsoil)$,

where B is the relative increase in flux with soil temperature, A describes flux when $Tsoil$ = 0, and $Q10 = exp(10*B)$.

Model fitting was performed using "JAGS" in R to calculate the posterior distribution with the Markov Chain Monte Carlo (MCMC) estimation. We used three chains with different starting values (A: 0.5, 0.6, 0.4; B: 0.2, 0.1, 0.15) and a burn-in of 3,000 iterations. Convergence was assessed using the Gelman and Rubin convergence diagnostic. We used a gamma likelihood distribution, with Eq. 1 as the mean, and *Beta* as the shape parameter (6, 7, 8; respectively). We used uninformative priors, ~dgamma(0.001, 0.001), for parameters *A*, *B*, and *Beta*. Model fit was evaluated using posterior predictive checks on the mean, standard deviation, and discrepancy between observations and predictions (Bayesian p-values: 0.50, 0.51, 0.57 respectively). We used the mean and standard deviation of the posterior predictive distribution (*i.e.*, predictions of new data by making a draw from the data model at each iteration of the MCMC chain, conditional on the current value of the parameters) at each observation of soil temperature to predict winter flux. The Q10 results are presented as median and 95% credible intervals.

Boosted regression tree analysis

We used boosted regression tree analysis (BRT) to model the drivers of winter CO_2 emissions and to upscale emissions to the pan-Arctic region under current and future climate scenarios. We used BRT because this machine learning method is capable of handling nonlinear and high-order interactions; is relatively insensitive to collinearity among predictors; can handle predictors that are continuous or categorical; and allows for missing predictor data[26]. The BRT model was fit in R[27] using 'gbm' package version 2.1.1[28], and using code adapted from[29]. Detailed description of the application of BRT to ecological data can be found in[26,29]. The BRT models were fitted with the following metaparameters: Gaussian error distribution, bag-fraction (*i.e.*, proportion of data used in each iteration) of 0.5, learning rate (*lr*; contribution of each tree to the final model) of 0.005, and a tree complexity (*tc*, maximum level of interactions) of two. We used 10-fold cross-validation (CV) to determine the optimal number of trees to achieve minimum predictive error and to fit the final model to the data.

We used geospatial data described above as input variables in our BRT model. Several of these variables were highly correlated because they were derived from the same data (*e.g.*, 16-year average max/mean EVI and max/mean EVI from the prior growing season) or were functionally similar data from different sources (*e.g.*, air temperature from WorldClim or MERRA-2). We removed highly correlated variables from the models (Spearman $\rho = 0.7$), retaining the variable within each functional category (*e.g.*, air temperature) that had the highest correlation with winter flux. We further reduced the model by removing variables in reverse order of their relative influence, until further removal resulted in a 2% average increase in predictive deviance. Relative influence estimates are based on the number of times a variable in the BRT model was selected for splitting, weighted by the squared improvement to the model as a result of each split, and averaged over all trees. Relative influence values were scaled so that all variables summed to 100[29]. We also removed variables that had a relative influence of less than 5% and that had a functional relationship with winter CO_2 flux that was contrary to prior expectations, potentially a result of model overfitting.

We compared this model using geospatial data as input variables with an alternative 'Site' model in which we also included *in situ* data as explanatory variables. Metrics of model fit (SI Table 6) were similar between models. We also found that when we compared the modeled flux estimates from the 'Spatial' and 'Site' BRT models, the estimates did not differ significantly ($\alpha = 0.05$). Therefore, we used the geospatial model in our final analysis because it allowed us to upscale results and project future fluxes. Inputs to the final models are in SI Figure 1 and SI Table 8.

We assessed BRT model performance using: 1. The correlation between predicted and observed values using the CV data (*i.e.*, data withheld from model fitting), hereafter referred to as the CV correlation, and; 2. deviance explained by the model over the evaluation dataset (*i.e.*, CV data), calculated as: % deviance = (CV null deviance - CV residual deviance)/CV null deviance *100.

Spatial and temporal domain for mapping

We scaled the modeled flux data to the northern permafrost land area ≥ 49°N[14], which comprises 16.95 × 10^6 km^2 of tundra and boreal lands (excludes glaciers, ice sheets and barren lands; Figure 1) with lake area removed. We defined the winter period as the months of October through April, encompassing combined winter and shoulder seasons (late autumn and early spring, e.g., October and April). Because the climate within this timeframe varies substantially across the northern permafrost region, this month-based definition, while temporally consistent, may include some areas that are influenced by climate that would fall outside expected winter temperature ranges. Therefore, we also explored defining the winter season based on soil temperature from MERRA-2 (soil layer 1) as the period when monthly mean soil temperature was below 0° C. The spatial extent of the modeled domain was variable across years when applying the temperature-based definition of winter; therefore, we use the fixed time period winter (October - April) to examine changes in winter CO_2 fluxes under future climate scenarios and in cross-model comparisons. Estimated winter emissions using the temperature-defined winter period, which included September and May for some locations, was 5% greater than emissions estimated for the full permafrost domain for the time period October through April.

Comparison of BRT estimates with process-based models

We compared our regional winter flux estimates to: 1) outputs from five process-based terrestrial models estimated for the northern permafrost domain: National Center for Atmospheric Research (NCAR) Community Land Model (CLM) versions 4.5 and 5; Lund-Potsdam-Jena Dynamic Global Vegetation Model (LPJ-DGVM), Wald Schnee und Landscraft version (LPJ-wsl); CARbon DAta MOdel FraMework (CARDAMOM); and the NASA SMAP Level 4 Carbon (L4C) Version 3 NATURE product; 2) estimates for the northern permafrost domain derived from FluxCom, a global gridded machine-learning NEE product; and 3) four process-based terrestrial models and eight atmospheric inversion models from the high latitude model intercomparison for the Regional Carbon Cycle Assessment and Processes (RECCAP) tundra and northern boreal domain[30].

For this application, CLM V4.5 and 5 with dynamic nitrogen and biogeochemistry were run at 0.5° resolution for > 40°N[31,32]. The CLM model has 10 soil layers and features dynamic vertical soil water flux. Soil carbon turnover is based on the Century decomposition model[33]. The two versions of the model utilize the same surface dataset, including plant functional type fraction. The forcing data used for CLM are NCAR Global Soil Wetness Project V3 fields from 1901 to 2014. The model components are run at a half-hourly time step and simulations are output to monthly averages. Model results for this study were analyzed for years 2003 to 2014.

The LPJ-wsl model includes an eight-layer soil freeze-thaw scheme and one-layer snow model in conjunction with a two-layer bucket model for hydrology[34]. Soil and litter decomposition in the LPJ model are driven by seasonal soil temperature and moisture status; soil temperature functions for respiration use a modified Arrhenius function[35]. Inputs to the LPJ-wsl model are from the NASA Global Modeling and Assimilation Office (GMAO) reanalysis record at 0.5 x 0.66° and monthly outputs. The model spin-up period is 1,400 years, and the model outputs are provided at 0.5° for years 2003 to 2017 to correspond with the BRT results.

The CARDAMOM outputs were obtained for years 2003 through 2010 from global 1° model-data fusion analysis and includes an aggregated canopy model to provide GPP, the Data Assimilation Linked Ecosystem Carbon model version 2 (DALEC2) for soil carbon flux, and a MCMC MDF algorithm[36]. Model inputs include global soil data and MODIS LAI time series. The MCMC model simulations apply a range of conditions on carbon pool turnover and carbon allocation ratios to constrain ecosystem variable interdependencies.

The NASA SMAP L4C product provides daily 9 km resolution estimates of NEE, GPP and ecosystem respiration using coupled soil decomposition and terrestrial carbon flux models calibrated against global FLUXNET tower CO_2 flux measurements[21]. The baseline L4C model is driven by NASA GMAO reanalysis daily surface meteorology and MODIS satellite vegetation data. Soil respiration is regulated using a three-pool decomposition model with cascading SOM decomposition rates for metabolic, structural, and recalcitrant components. Litterfall carbon inputs to the soil model are defined as a prescribed fraction of daily NPP calculated from a satellite based light-use efficiency model. Soil heterotrophic respiration is regulated by pool size, decomposition rate parameters, soil temperature and soil water content. Outputs from NASA SMAP L4C were compared with this study for the years 2003 to 2017.

FluxCom is a gridded ensemble of NEE CO_2 fluxes, generated by upscaling FLUXNET site observations using machine learning techniques, gridded meteorological data, and MODIS remote sensing[37]. FluxCom is available at a 0.5° spatial resolution, spanning 1980 to 2013; we used monthly averaged output in this analysis. There are some key differences between FluxCom and the machine learning model used in this study: 1) FluxCom is a global product, while our model was developed specifically for the northern permafrost domain using only high latitude flux data collected during the non-growing season; 2) In addition to MODIS, we included AMSR surface moisture data and predictors specifically relevant to permafrost regions (*e.g.*, permafrost zonation index, northern soil carbon stock, tundra and boreal land cover); 3) For the northern latitudes, the data used to train FluxCom spanned 1991-2007, while our dataset extended through 2017; and 4) Our dataset included >100 sites, while FluxCom included 25 sites in the northern permafrost region.

Finally, we also compare our BRT CO_2 emissions estimates with the RECCAP high latitude model intercomparison results[30]. The models evaluated here include four process-based models (LPJ-Guess, Orchidee, TEM6, and TCF) and 8 inversion models (C13_CCAM_law, C13_MATCH_rayner, JENA_s96_v3.3, JMA_2010, LSCE_an_v2.1, LSCE_var_v1.0, NICAM_niwa_woaia, rigc_patra).

Projected winter CO_2 flux

Inputs for the BRT model of future scenarios of winter CO_2 flux were obtained from ensembles of Earth System Model (ESM) outputs from the Fifth Coupled Model Intercomparison Project (CMIP5)[38]. Inputs included: 1) Annual GPP; 2) Mean annual summer LAI (July & August); 3) Mean summer soil moisture (June, July, August); 4) Mean monthly soil moisture; 5) Mean monthly near-surface (2 m) air temperature; and 6) Mean monthly soil temperature (layer 1) (SI Table 7). Although total summer precipitation (June, July, August) was not included in our winter CO_2 projection model, we obtained future projections of precipitation as a reference to explain trends in surface soil moisture. Outcomes from two representative concentration pathways (RCP), RCP 4.5 and 8.5, were used as inputs for the future winter CO_2 emission scenarios. RCP 4.5 assumes a peak in greenhouse gas emissions around 2040; emissions in RCP 8.5 continue to rise during the 21st century[38]. The ensemble mean RCP 4.5 and 8.5 predictor fields were bias-corrected using the delta, or perturbation method[39], based on historic ESM outputs and observed historical data and reprojected to EASE2 25 km grids.

To obtain an estimate of aggregated model uncertainty for the permafrost domain, we first used an average of the internal root mean squared error (RMSE; g C m^{-2} d^{-1}) from 1,000 BRT ensemble runs, with the models trained using our *in situ* winter flux database. We then made the assumption that the RMSE (0.21 g C m^{-2} d^{-1}) applied equally to all grid cell area within the domain. This provided us with a total region error budget of 813 Tg C for the winter period.

In addition to our RMSE based uncertainty estimate, we also examined the inherent variability in the ensemble fitting of the regression trees based on subsets of training data and external (withheld) validation data. To do this, we followed the approach of[40]. Bootstrapped BRT model simulations were obtained for the baseline 2003-2017 winter (October - April) climatology and for decadal non-growing season climatologies bracketed from 2017 through 2100. The flux means and 95% confidence intervals (CIs) were obtained for each grid cell using output from 1,000 bootstrap BRT model runs where 30% of the *in situ* data were removed during each simulation for validation purposes. We used the resulting 95% CIs to provide additional estimates of model uncertainty; this ranged from 50 to 66 Tg C $winter^{-1}$ across the 2003 through 2100 period, with higher model uncertainty occurring under the more extreme future temperature scenarios.

For the CMIP5 RCP 4.5 and 8.5 simulations of respiration, we use an r1i1p1ensemble mean from the following models: CanESM2, GFDL-ESM2M, GISS-E2-H-CC, GIS-E2-H, GISS-E2-R, GISS-E2-R-CC, inmcm4, IPSL-CM5A-LR, IPSL-CM5A-MR, MIROC-ESM, MIROC-ESM-CHEM, MPI-ESM-LR, MPI-ESM-MR, NorESM1-M, NorESM1-ME[38].

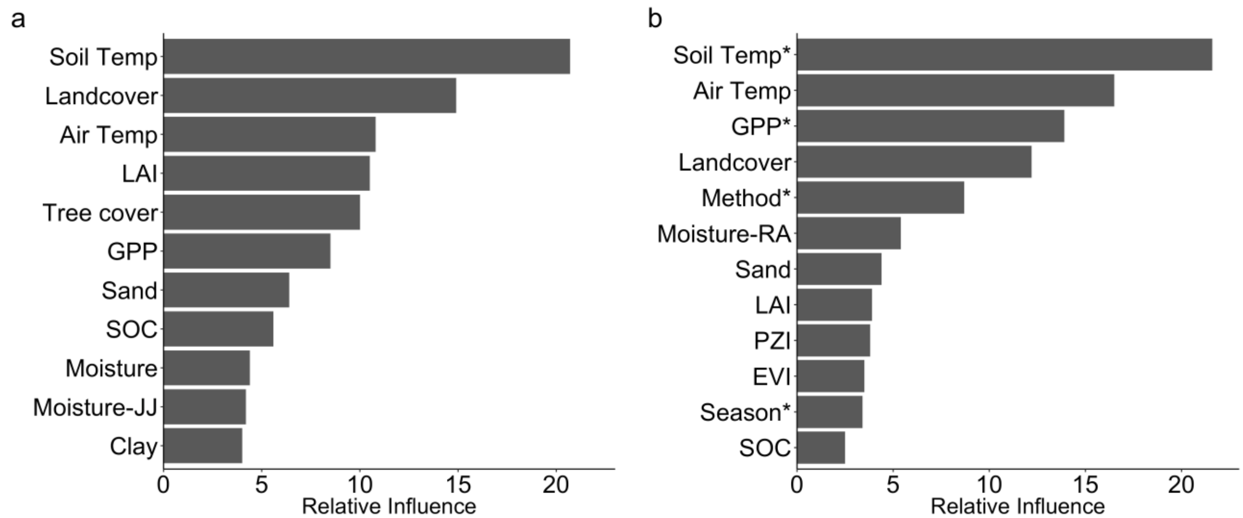

SI Figure 1. Drivers of winter CO_2 flux based on relative influence of predictor variables in the boosted regression tree model. Panel (a) shows geospatial inputs for the final model used in this study. For comparison, we also ran an alternative 'Site' model that incorporated both *in situ* and geospatial data as input variables (b). The *in situ* data that were retained in the final model are marked with an asterisk. Variable descriptions are in the text and in SI Table 8.

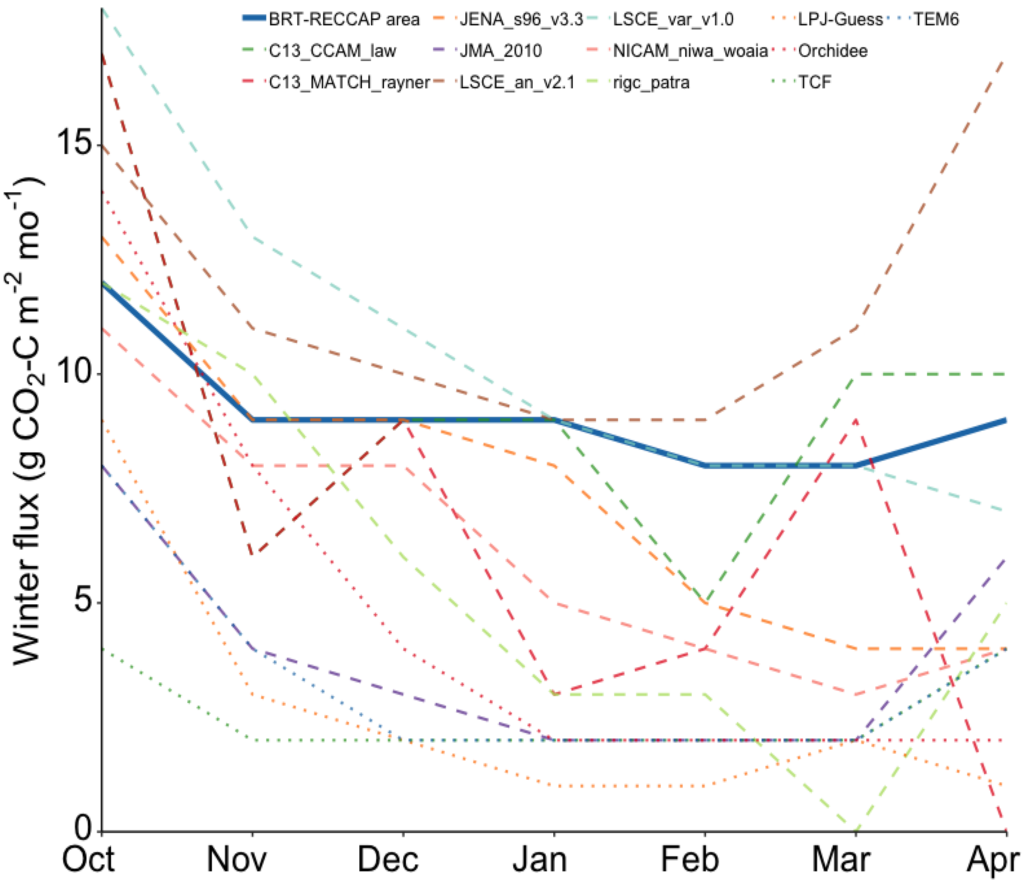

SI Figure 2. Average monthly CO_2 fluxes estimated from the boosted regression tree (BRT) analysis (solid blue line) compared with winter net ecosystem CO_2 exchange from four process-based models ('bottom-up estimate'; dotted lines) and eight inversion models ('top-down'; dashed lines) for the Global Carbon Project's REgional Carbon Cycle Assessment and Processes (RECCAP) tundra and northern boreal domain. The winter fluxes are estimated for the time interval of 2003 to 2017 for BRT, ranging between 1985 - 2009 for inversion models, and 1990-2006 for process models.

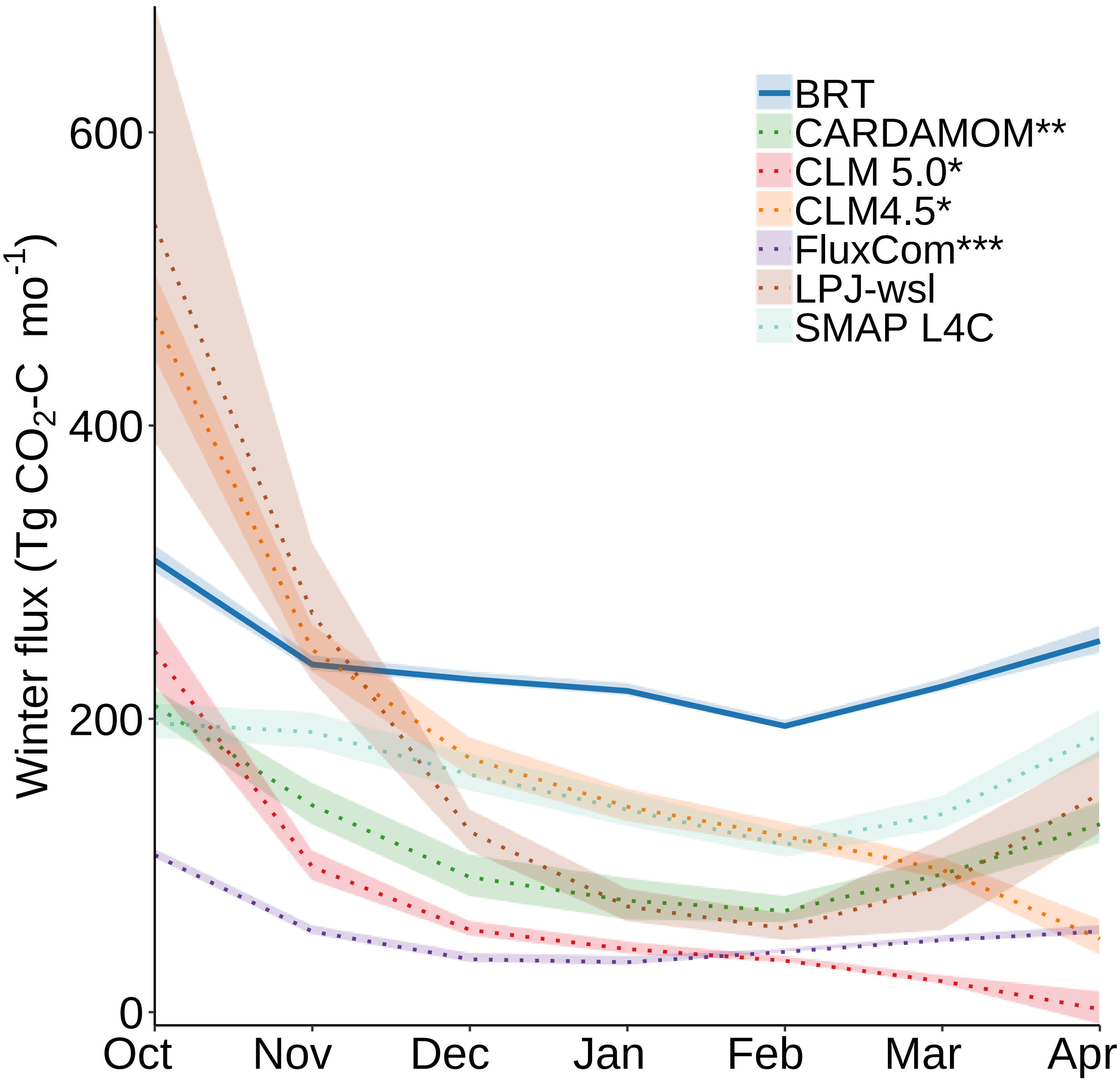

SI Figure 3. Monthly CO_2 flux (and standard deviation representing interannual variability) estimated for the permafrost region (17×10^6 km^2) from the boosted regression tree (BRT) model (solid blue line) and winter CO_2 flux outputs (NEE) from five terrestrial process models and FluxCom. Fluxes are annual averages of the years 2003 to 2017 (BRT, LPJ, SMAP), 2003 to 2014 (CLM 4.5, CLM 5), 2003 to 2010 (CARDAMOM), and 2003 to 2013 (FluxCom).

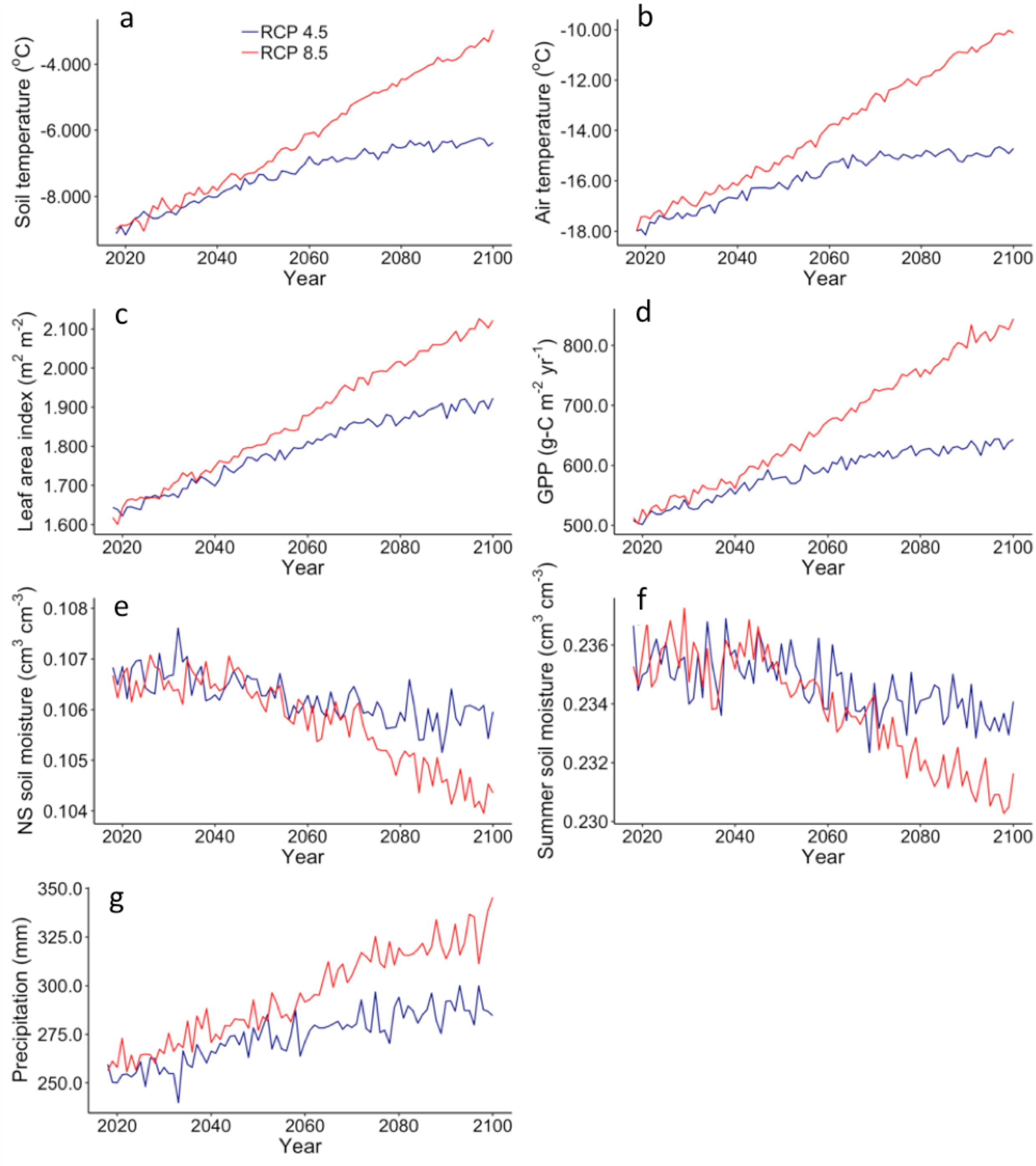

SI Figure 4. Projected (a) mean winter (Oct-April) soil temperature, (b) mean winter air temperature, (c) mean leaf area index (July-August), (d) annual gross primary productivity (GPP), (e) mean non-summer (NS; September - May) unfrozen soil moisture, (f) mean summer soil moisture (June-August), and (g) cumulative summer precipitation (June-August) for the northern permafrost region from 2018 through 2100 under RCP 4.5 (blue) and 8.5 (red) based on ESM ensemble outputs.

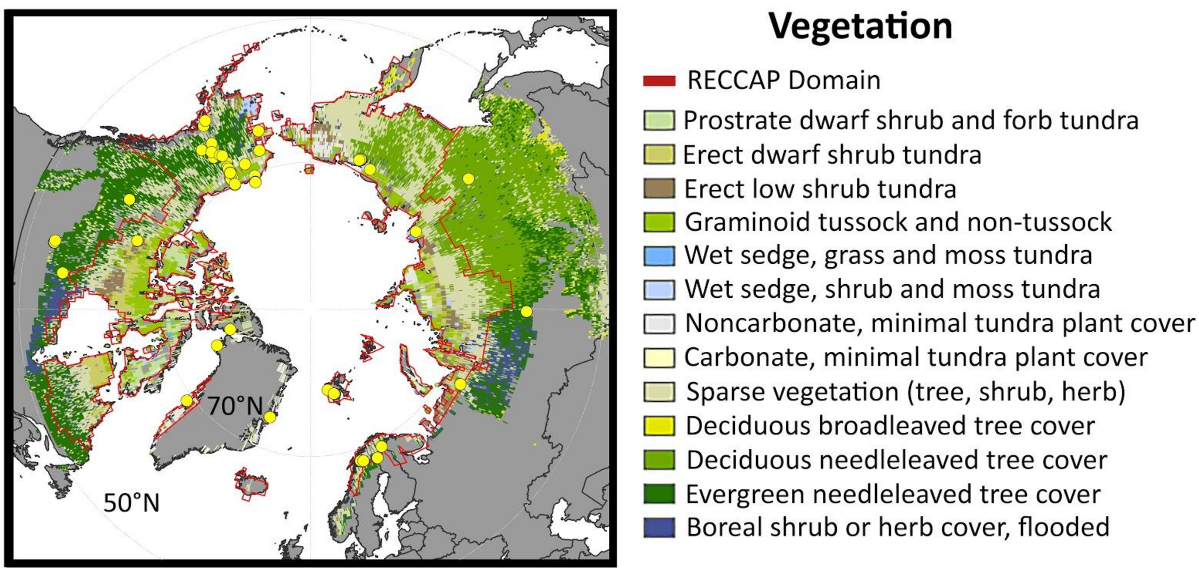

SI Figure 5. Locations of synthesized *in situ* winter CO_2 flux data (yellow circles) and dominant landcover types within the study region, which includes boreal deciduous and evergreen forests, and flooded wetlands. Tundra regions include wet sedge, shrub-lands, and graminoid dominated vegetation. Landcover classifications were derived from the Circumpolar Arctic Vegetation Map for tundra sites and the European Space Agency Climate Change Initiative V.2 land cover classifications for boreal sites. The REgional Carbon Cycle and Assessment Processes (RECCAP) domain is outlined in red.

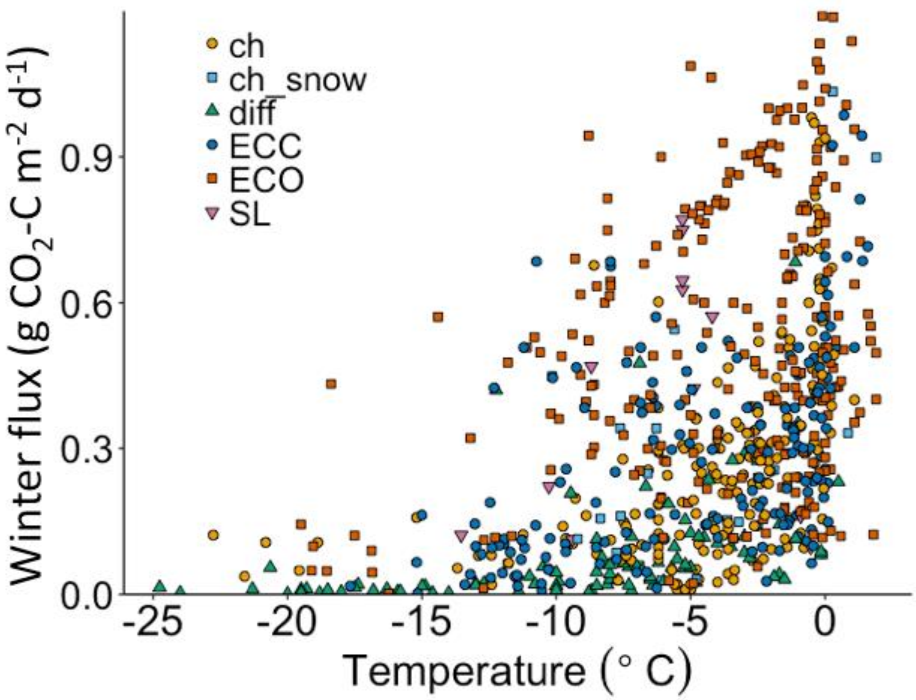

SI Figure 6. Soil temperature distribution of winter CO_2 flux data in this synthesis, which included data collected using six measurement methods: chamber (ch), chamber placed atop the snow pack (ch_snow), diffusion (diff), eddy covariance-closed path (ECC), eddy covariance-open path (ECO), and soda lime (SL). Note that this figure is based on a subset (74%) of the 1,014 flux data where soil temperature data were available. Each point represents one site-month of CO_2 flux/temperature data.

SI Table 1. Summary of sites in the flux synthesis. Location description includes key words to distinguish sampling locations with a site. Landcover (LC) descriptions are in SI Table 4. Measurement methods, which are further described in the supplemental text, include chamber placed on top of ground (C), chamber on top of snow pack (CS), diffusion through the snowpack (D), eddy covariance-open path (ECO), eddy covariance-closed path (ECC), and soda lime (SL). Permafrost (Perm) zones include: isolated/sporadic (I-S), discontinuous (D), continuous (C)[14]. Temperatures are average annual temperature (1960-1990) from the WorldClim database[6]. The number of winter flux sites representing individual LC types are: ENLF (24); BDF (5); BSW (14); CMC (7); DNF (8); G1 through G4 (20); NMC (9); P2 (4); S1 (13); S2 (16); SBV (20); W1 (7); W2 (6): see SI Table 4 for landcover definitions.

Lat	Long	Location description	Country	Biome	LC	Perm	Method	Temp	Ref
53.88	-104.65	BOREAS, Young jack pine	Canada	Boreal	ENLF	I-S	CS	-0.5	[41]
53.92	-104.69	BOREAS, Old jack pine	Canada	Boreal	ENLF	I-S	CS	-0.6	[41]
53.99	-105.12	BOREAS, Old black spruce	Canada	Boreal	ENLF	I-S	CS	-0.9	[41]
55.9	-98.40	BOREAS, Fen	Canada	Boreal	BSW	I-S	ECC	-3.2	[42]
60.71	-150.89	Kenai Lowlands, Moss	USA	Boreal	BSW	I-S	D	1.6	[43]
60.71	-150.89	Kenai Lowlands, Sedge	USA	Boreal	BSW	I-S	D	1.6	[43]
60.71	-150.89	Kenai Lowlands, Shrub	USA	Boreal	BSW	I-S	D	1.6	[43]
60.71	-150.89	Kenai Lowlands, Small tree	USA	Boreal	SBV	I-S	D	1.6	[43]
60.75	89.38	Zotino, Central Siberia, Bog	Russia	Boreal	BSW	I-S	ECC	-2.8	[44]
60.75	89.39	Zotino, Central Siberia, Pinus forest	Russia	Boreal	ENLF	I-S	ECC	-2.8	[45]
61.2	-149.82	Anchorage, AK, Upland boreal forest	USA	Boreal	ENLF	I-S	D	1.9	[46]
61.31	-121.3	Scotty Creek, Bog	Canada	Boreal	BSW	I-S	ECO	-3.5	[47]
61.31	-121.3	Scotty Creek, Forest-wetland	Canada	Boreal	SBV	I-S	ECC	-3.5	[47]
62.26	129.62	Yakutsk, Larch forest, Grass	Russia	Boreal	DNF	C	ECC	-10.8	[48]
63.88	-149.25	Eight Mile Lake, AK, EC tower	USA	Tundra	SBV	D	ECO	-4.1	[49,50], *U1**
63.88	-149.25	Eight Mile Lake, AK, Minimal thaw	USA	Tundra	SBV	D	C	-4.1	[51,52]
63.88	-149.25	Eight Mile Lake, AK, Moderate thaw	USA	Tundra	SBV	D	C	-4.1	[51,52]
63.88	-149.25	Eight Mile Lake, AK, Extensive thaw	USA	Tundra	SBV	D	C	-4.1	[51,52]
63.88	-149.23	Eight Mile Lake, AK, CiPEHR control	USA	Tundra	SBV	D	C, SL	-4.2	[4,53,54]
63.9	-145.67	Delta Junction, AK, Deciduous forest	USA	Boreal	BDF	D	ECO	-3.2	[55]
63.9	-145.67	Delta Junction, AK, Evergreen forest	USA	Boreal	ENLF	D	ECO	-3.2	[55]
64.41	-148.19	Bonanza Creek, AK, Permafrost plateau	USA	Boreal	ENLF	D	C	-3	[56]

Lat	Long	Location description	Country	Biome	LC	Perm	Method	Temp	Ref
64.41	-148.19	Bonanza Creek, AK, Bog	USA	Boreal	BSW	D	C, D, ECO	-3	[56,57]U2,U3
64.41	-148.19	Bonanza Creek, AK, Black spruce forest	USA	Boreal	ENLF	D	ECO	-3	[57], U2
64.41	-148.19	Bonanza Creek, AK, Fen	USA	Boreal	BSW	D	ECO	-3	[57], U2
64.75	-148.75	Bonanza Creek, AK, Muskeg	USA	Boreal	BSW	D	SL	-3.8	[58]
64.8	-147.87	Bonanza Creek, AK, Black spruce forest	USA	Boreal	ENLF	D	C	-2.8	[59]
64.83	-111.63	Daring Lake, Birch hummock	Canada	Tundra	S1	C	C, SL	-10.8	[60,61], U4
64.86	-163.71	Council, AK, Tundra sphagnum	USA	Tundra	S2	D	C	-4	[62]
64.86	-163.71	Council, AK, Tundra lichen	USA	Tundra	S2	D	C	-4	[62]
64.86	-163.71	Council, AK, Tundra tussock	USA	Tundra	S2	D	C	-4	[62]
64.87	-147.85	Fairbanks, AK, Black spruce forest	USA	Boreal	ENLF	D	CS, D	-2.9	[63,64]
64.87	-111.58	Daring Lake, Wet sedge	Canada	Tundra	W1	C	SL	-11.1	[60]
64.87	-111.58	Daring Lake, Dry heath	Canada	Tundra	S1	C	SL	-11.1	[60]
64.87	-111.58	Daring Lake, Tall birch understory	Canada	Tundra	S2	C	SL	-11.1	[60]
64.87	-147.85	Fairbanks, AK, Black spruce forest	USA	Boreal	ENLF	D	ECO	-2.9	[65]
65.64	-147.47	Fairbanks, AK, Old black spruce	USA	Boreal	ENLF	D	C	-5.5	[66]
65.84	-149.65	Interior AK, Lower Yukon black spruce	USA	Boreal	ENLF	D	C	-5.8	[11]
66.08	-150.17	Interior AK, Upper Yukon black spruce	USA	Boreal	ENLF	D	C	-5.3	[11]
67.18	-150.31	Coldfoot, AK, Young black spruce	USA	Boreal	ENLF	C	C	-7.5	[11,66]
67.38	63.37	Lek Vorkuta, Intermediate lawn	Russia	Tundra	S2	D	D	-6.5	[67]
67.38	63.37	Lek Vorkuta, Hummock	Russia	Tundra	S2	D	D	-6.5	[67]
67.38	63.37	Lek Vorkuta, Wet lawn	Russia	Tundra	S2	D	D	-6.5	[67]
67.38	63.37	Lek Vorkuta, Intermediate flark	Russia	Tundra	S2	D	D	-6.5	[67]
67.38	63.37	Lek Vorkuta, Wet flark	Russia	Tundra	S2	D	D	-6.5	[67]
67.48	-162.2	Agashashok River, NTL-Low density (LD) spruce	USA	Boreal	ENLF	C	D	-7.1	[68]
67.48	-162.2	Agashashok River, STL-LD white spruce	USA	Boreal	ENLF	C	D	-7.1	[68]
67.48	-162.2	Agashashok River, SNE, White spruce	USA	Boreal	ENLF	C	D	-7.1	[68]

Lat	Long	Location description	Country	Biome	LC	Perm	Method	Temp	Ref
67.48	-162.2	Agashashok River, SNE, White spruce forest	USA	Boreal	ENLF	C	D	-7.1	[68]
67.48	-162.2	Agashashok River, NSE, White spruce forest	USA	Boreal	ENLF	C	D	-7.1	[68]
67.48	-162.2	Agashashok River, NNE, White spruce	USA	Boreal	ENLF	C	D	-7.1	[68]
67.48	-162.2	Agashashok River, SSE, White spruce forest	USA	Boreal	ENLF	C	D	-7.1	[68]
67.48	-162.2	Agashashok River, TER, LD white spruce	USA	Boreal	ENLF	C	D	-7.1	[68]
67.74	-149.76	Interior AK, Gold Creek white spruce	USA	Boreal	ENLF	C	C	-8.8	[11]
67.99	-149.76	Brooks Range, AK, Tundra-boreal ecotone	USA	Boreal	SBV	C	C	-10.1	[66,69]
68.00	24.21	Lompolojänkkä, Nutrient-rich fen	Finland	Boreal	BSW	D	ECC	-2	[70]
68.18	-149.44	North Slope, AK, Subalpine tundra	USA	Tundra	S1	C	C	-11.7	[11,66]
68.3	18.82	Abisko	Sweden	Tundra	SBV	I-S	C	-1.9	[71]
68.33	19.17	Vuoskojaiveh, Birch	Sweden	Boreal	BDF	D	C	0	[72]
68.33	19.17	Vuoskojaiveh, Heath	Sweden	Tundra	SBV	D	C	0	[72]
68.33	18.5	Latnjajaure, Heath snowbed	Sweden	Tundra	SBV	D	D	-2.2	[2,73]
68.33	18.5	Latnjajaure, Meadow snowbed	Sweden	Tundra	SBV	D	D	-2.2	[2,73]
68.33	18.5	Latnjajaure, Heath shallow	Sweden	Tundra	SBV	D	D	-2.2	[2,73]
68.33	18.5	Latnjajaure, Meadow shallow	Sweden	Tundra	SBV	D	D	-2.2	[2]
68.33	18.5	Latnjajaure, Mesic meadow	Sweden	Tundra	SBV	D	D	-2.2	[73]
68.35	18.84	Abisko, Heath control	Sweden	Tundra	SBV	D	C	-0.1	[72,74,75]
68.35	18.84	Abisko, Birch control	Sweden	Boreal	BDF	D	C	-0.1	[72,74,75]
68.35	18.82	Abisko, Control	Sweden	Tundra	SBV	D	C	-0.1	[76]
68.37	19.05	Stordalen, Mire	Sweden	Boreal	BSW	D	ECO	0.1	[77]
68.43	18.55	Paktajaure, Birch	Sweden	Boreal	BDF	D	C	-0.5	[72]
68.43	18.55	Paktajaure, Heath	Sweden	Tundra	SBV	D	C	-0.5	[72]
68.43	18.27	Vassijaure, Birch	Sweden	Boreal	BDF	D	C	-0.1	[72]
68.43	18.27	Vassijaure, Heath	Sweden	Tundra	SBV	D	C	-0.1	[72]
68.49	-155.75	Ivotuk, AK	USA	Tundra	G4	C	ECC	-11.6	U5
68.61	-149.31	Imnavait Creek, AK, Wet sedge	USA	Tundra	W2	C	C, ECO	-11.9	[78-80]

Lat	Long	Location description	Country	Biome	LC	Perm	Method	Temp	Ref
68.61	-149.3	Imnavait Creek, AK, Tussock	USA	Tundra	G4	C	C, ECO	-12.1	[78,79]
68.61	-149.3	Imnavait Creek, AK, Heath	USA	Tundra	S1	C	C, ECO	-12.2	[78-80], U6
68.62	161.34	Cherskiy, NE Siberia, Floodplain	Russia	Boreal	BSW	C	ECC	-12.4	[81]
68.62	-149.61	Toolik Lake, AK, Tussock tundra	USA	Tundra	G4	C	D	-11.3	[46], U7
68.63	-149.63	Toolik Lake, AK, Dry tundra	USA	Tundra	S1	C	D, SL	-11.4	[82], U7
68.63	-149.6	Toolik Lake, AK, Wet sedge tundra	USA	Tundra	W2	C	D	-11.3	U7
68.63	-149.6	Toolik Lake, AK, Riparian willow tundra	USA	Tundra	S2	C	D	-11.3	U7
68.63	-149.56	Toolik Lake, AK, Non-acidic tundra	USA	Tundra	G4	C	SL	-11.5	[58]
68.63	-149.56	Toolik Lake, AK, Dry heath tundra	USA	Tundra	S1	C	SL	-11.5	[58]
68.63	-149.56	Toolik Lake, AK, Shrub tundra	USA	Tundra	S2	C	SL	-11.5	[58]
68.63	-149.56	Toolik Lake, AK, Tussock tundra	USA	Tundra	G4	C	SL	-11.5	[58]
68.63	-149.57	Toolik Lake, AK, Dwarf birch tundra	USA	Tundra	S1	C	D	-11.5	U7
68.63	-149.63	Toolik Lake, AK, Heath	USA	Tundra	S1	C	D	-11.4	[83]
68.63	-149.63	Toolik Lake, AK, Snow drifts	USA	Tundra	G4	C	D	-11.4	[83]
68.63	-149.63	Toolik Lake, AK, Tussock	USA	Tundra	G4	C	D	-11.4	[83]
68.63	-149.63	Toolik Lake, AK, Cassiope	USA	Tundra	S1	C	D	-11.4	[83]
68.63	-149.63	Toolik Lake, AK, Riparian	USA	Tundra	S2	C	D	-11.4	[83]
68.63	-149.63	Toolik Lake, AK, Moist tundra	USA	Tundra	G4	C	D, SL	-11.4	[82]
68.63	-149.58	North Slope, AK, Tussock	USA	Tundra	G4	C	C	-11.4	[84]
68.7	161.55	Cherskiy, Larch forest, low density	Russia	Boreal	DNF	C	C	-13	U8
68.72	161.53	Cherskiy, Post-fire shrub	Russia	Boreal	DNF	C	C	-12.9	U8
68.73	161.4	Cherskiy, Old larch forest	Russia	Boreal	DNF	C	C	-12.5	U8
68.74	161.4	Cherskiy, Larch forest	Russia	Boreal	DNF	C	D	-12.6	[85]
68.74	161.41	Cherskiy, Larch, moss/lichen/shrub	Russia	Boreal	DNF	C	D	-12.6	[86]
68.74	161.41	Cherskiy, Larch forest, graminoid	Russia	Boreal	DNF	C	D	-12.6	[86]
68.75	161.45	Cherskiy, Dense larch stand	Russia	Boreal	DNF	C	C	-12.8	U8
68.75	161.33	Cherskiy, Floodplain tundra	Russia	Tundra	BSW	C	ECC	-12.6	U9
68.81	161.99	Kallercha, Tundra	Russia	Tundra	SBV	C	C	-12.6	[87]

Lat	Long	Location description	Country	Biome	LC	Perm	Method	Temp	Ref
68.84	-149.84	Toolik Lake, AK, Heath	USA	Tundra	S1	C	D	-11.5	[88]
68.84	-149.84	Toolik Lake, AK, Tussock	USA	Tundra	G4	C	D	-11.5	[88]
68.91	-148.88	North Slope, AK, Upland tundra	USA	Tundra	G4	C	C	-10.3	[66,69]
69.13	27.28	Kaamanen, Mesotrophic fen	Finland	Boreal	BSW	I-S	ECC	-1.1	[89,90]
69.15	-148.85	North Slope, AK, Tussock tundra	USA	Tundra	G4	C	C	-10.4	[84]
69.15	-148.85	Happy Valley, AK, Shrub tundra	USA	Tundra	S1	C	C	-10.4	[91]
69.15	-148.85	Happy Valley, AK, Acidic tundra	USA	Tundra	G4	C	C	-10.4	[91]
69.25	-53.51	Disko Island, Arctic Station	Greenland	Tundra	NMC	C	C, ECC	-5.5	U4, U10
69.28	-148.47	Happy Valley, AK, Tussock	USA	Tundra	G4	C	D	-10.9	[83]
69.28	-148.47	Happy Valley, AK, Riparian	USA	Tundra	S2	C	D	-10.9	[83]
69.42	-148.7	Sagwon, AK, Acidic tussock tundra	USA	Tundra	G4	C	SL	-10.8	[58]
69.49	156.99	Akhmelo, Sedge marsh	Russia	Tundra	G3	C	C	-13.4	[87]
69.49	-148.81	Kuparuk Watershed, AK, Riparian	USA	Tundra	S2	C	D	-10.5	[92]
69.49	-148.81	Kuparuk Watershed, AK, Coastal Plain	USA	Tundra	G4	C	D	-10.5	[92]
69.49	-148.81	Kuparuk Watershed, AK, Upland tussock	USA	Tundra	G4	C	D	-10.5	[92]
69.49	-148.81	Kuparuk Watershed, AK, Water track	USA	Tundra	S2	C	D	-10.5	[92]
69.5	-149.5	Sag River, AK, Shrub	USA	Tundra	S2	C	D	-11	[83]
69.84	-148.71	North Slope, AK, Coastal tundra	USA	Tundra	S1	C	C	-10.8	[11]
69.93	-148.82	24-mile, AK, Nonacidic tundra	USA	Tundra	W2	C	C	-10.8	[91]
70.27	-148.88	North Slope, AK, Coastal wet sedge	USA	Tundra	W2	C	C	-11.3	[84]
70.27	-148.88	Prudhoe Bay, AK, Alaska	USA	Tundra	W2	C	ECC	-11.3	[93]
70.28	-148.88	North Slope, AK, Coastal wet sedge	USA	Tundra	G4	C	C	-11.2	[84,91]
70.38	-148.75	North Slope, AK, Moist acidic tundra	USA	Tundra	W2	C	D	-11.4	[83]
70.47	-157.41	Atqasuk, AK, Moist acidic tundra	USA	Tundra	W1	C	ECO, ECC	-11.2	[94], U5
71.28	-156.6	Utqiaġvik (Barrow), AK, BES	USA	Tundra	W1	C	ECC	-12.3	U5
71.28	-156.61	Utqiaġvik (Barrow), AK, BEO	USA	Tundra	W1	C	ECC	-12.3	U5
71.32	-156.61	Utqiaġvik (Barrow), AK, CDML	USA	Tundra	W1	C	ECC	-12.3	U5
72.37	126.5	Samoylov Island, Wet polygonal tundra	Russia	Tundra	S1	C	ECC	-14.7	U11

Lat	Long	Location description	Country	Biome	LC	Perm	Method	Temp	Ref
74.47	-20.58	Zackenberg, Dry heath	Greenland	Tundra	NMC	C	C	-10.5	[95,96], U4
74.48	-20.54	Zackenberg, Heath, DK-ZaH	Greenland	Tundra	NMC	C	C, ECC	-10.5	U4, U12
74.48	-20.54	Zackenberg, Salix heath	Greenland	Tundra	NMC	C	C	-10.5	U4
74.48	-20.56	Zackenberg, Fen	Greenland	Tundra	NMC	C	D, C, CS, ECC	-14.2	[97,98], U12
76.53	-68.7	Pituffik Peninsula, Dwarf shrub tundra	Greenland	Tundra	NMC	C	SL	-11.3	[99]
78.17	16.1	Adventdalen, Svalbard, Mesic site	Norway	Tundra	CMC	C	C	-5.7	[100]
78.17	16.1	Adventdalen, Svalbard, Wet site	Norway	Tundra	CMC	C	C	-5.7	[100]
78.17	16.07	Adventdalen, Svalbard, Heath shallow	Norway	Tundra	CMC	C	C, D	-5.7	[2,101]
78.17	16.07	Adventdalen, Svalbard, Meadow shallow	Norway	Tundra	CMC	C	C, D	-5.7	[2,101]
78.17	16.07	Adventdalen, Svalbard, Dry heath	Norway	Tundra	CMC	C	C	-5.7	[102]
78.17	16.1	Adventdalen, Svalbard, Wet meadow	Norway	Tundra	CMC	C	SL	-5.7	[103]
78.17	16.1	Adventdalen, Svalbard, Mesic heath	Norway	Tundra	CMC	C	SL	-5.7	[103]
78.18	15.92	Adventdalen, Svalbard, Fen, polygons	Norway	Tundra	W1	C	D	-5.6	[98]
78.19	15.92	Adventdalen, Svalbard, eddy tower	Norway	Tundra	P2	C	ECC	-6	[104]
78.2	15.6	Endalen, Svalbard, Moist heath	Norway	Tundra	P2	C	C	-7.2	[10]
78.2	15.6	Endalen, Svalbard, Dry heath	Norway	Tundra	P2	C	C	-7.2	[10]
78.2	15.6	Endalen, Svalbard, Salix snow bed	Norway	Tundra	P2	C	C	-7.2	[10]
78.22	15.32	Björnedalen, Svalbard	Norway	Tundra	W1	C	C	-6	U13
78.9	-75.92	Alexandra Fjord, Nunavut, Mesic site	Canada	Tundra	NMC	C	SL	-16.4	[105]
78.9	-75.92	Alexandra Fjord, Nunavut, Dry site	Canada	Tundra	NMC	C	SL	-16.4	[105]
78.9	-75.92	Alexandra Fjord, Nunavut, Wet site	Canada	Tundra	NMC	C	SL	-16.4	[105]
78.92	11.95	Spitzbergen, Svalbard, Non-sorted circles	Norway	Tundra	G1	C	ECO	-5.2	[106]

* Lead providers of unpublished data: U1: Celis/Schuur; U2: Euskirchen; U3: Waldrop; U4: Christiansen; U5: Zona/Oechel; U6: Egan/Risk; U7: Sullivan; U8: Davydov; U9: Goeckede (data available at http://www.europe-fluxdata.eu/home/site-details?id=168); U10: Elberling; U11: Sachs; U12: Lund; U13: Friborg.

SI Table 2. Growing season (May-September), Winter (October-April), and Annual average CO_2 exchange (Tg C yr^{-1}) for the northern permafrost land area (17×10^6 km^2) during 2003-2017 (2003-2014 for CLM; 2003-2013 for FluxCom). Negative values indicate CO_2 uptake.

	Growing Season	**Winter**	**Annual**
LPJ-wsl	-1647	1296	-351
CLM 4.5	-787	1301	514
CLM 5.0	-687	503	-184
SMAP	-1017	1126	109
CARDAMOM	-1025	812	-213
FluxCom	-932	377	-555

SI Table 3. Temporal trends in winter CO_2 emissions (Tg C yr^{-1}) from the current permafrost region from 2018 through 2100. Kendall's correlation coefficient, τ, describes the strength of the time-series and Theil-Sen (TS) and ordinary least squares (OLS) slopes describe the rate of change in winter flux. Normalized OLS slopes account for differences in land area within each zone. All trends were significant ($p < 0.001$).

Zone	**Area (10^6 km^2)**	**τ**	**TS Slope (Tg C yr^{-1})**	**OLS slope (Tg C yr^{-1})**	**OLS-normalized (kg C km^{-2} yr^{-1})**
RCP 4.5					
Full domain	16.95	0.77	4.48	4.34	256
Continuous	9.25	0.81	2.33	2.31	250
Discontinuous	2.71	0.64	0.81	0.78	288
Sporadic	2.51	0.72	0.66	0.65	259
Isolated	2.48	0.76	0.60	0.60	242
RCP 8.5					
Full domain	16.95	0.89	8.27	8.29	489
Continuous	9.25	0.85	4.77	4.76	515
Discontinuous	2.71	0.92	1.42	1.42	524
Sporadic	2.51	0.91	1.13	1.14	454
Isolated	2.48	0.91	0.96	0.96	387

SI Table 4. Landcover vegetation types included in the boosted regression tree (BRT) model. Land cover classes were extracted from CAVM and ESA CCI maps based on site coordinates. Model count (CT) indicates the number of observations used to train the BRT model for each land cover type. Map CT indicates the number of 25 km equal area grid cells for each land cover type in the study domain.

Source	Code	Land Cover Description	Model CT	Map CT
CAVM	P2	Prostrate dwarf shrub and forb tundra	17	739
CAVM	S1	Erect dwarf shrub tundra	150	1166
CAVM	S2	Erect low shrub tundra	46	920
CAVM	G1-G4	Graminoid tussock and non-tussock (sedge, moss, minimal shrub)	112	2078
CAVM	W1	Wet sedge, grass and moss tundra	51	129
CAVM	W2	Wet sedge, shrub and moss tundra	81	413
CAVM	NMC	Noncarbonate mountain complex (barren; minimal plant cover)	84	723
CAVM	CMC	Carbonate mountain complex (barren; minimal plant cover)	51	33
CCI	SBV	Sparse boreal vegetation (tree, shrub, herb)	124	6922
CCI	BDF	Deciduous broadleaved forest, closed to open canopy	16	484
CCI	DNF	Deciduous needle leaf forest, closed to open canopy	64	7322
CCI	ENLF	Evergreen needle leaf forest, closed to open canopy	109	6952
CCI	BSW	Shrub or herb cover, flooded	138	1372
		Total	**1,043**	**29,253**

SI Table 5. Summary of incubation data. Incubation temperatures (Temp, C) reflect ranges for data used in this synthesis. Type/depth is the soil layer or depth of the soils incubated. Length is the incubation length (days) used to calculate CO_2 release.

Lat	Long	Site description	Type/depth	Length	Temp	Permafrost	Country	Ref
56.4* 64.17*	13.00* 19.58*	Pine/spruce forests, mire	Organic	10	-4	None	Sweden	[107]
68.33 68.35	18.83 18.67	Mesic dwarf shrub heath, Abisko Graminoid rich heath, Abisko	4-6 cm	4-18	-4, 2	Discontin.	Sweden	[108]
70.00* 64.7*	-149.00* -163.00*	27 tundra sites, Alaska	0-100 cm	14	-2	Continuous Discontin.	USA	[109]
74.47	20.57	Well-drained heath, Zackenberg	A-horizon	4-7	-18 to 2	Continuous	Greenland	[110]
68.63	-149.63	Wet sedge, tussock and shrub tundra, Toolik	Organic	20	-12 to 2	Continuous	USA	[111]
71.36 57.02 58.25	-156.63 82.58 140.50	Tussock tundra, Utqiaġvik, AK Peat bog, Plotnikovo Mesotrophic bog, Kopparrås mire	5-15 cm	NA	-39 to 0	Continuous None Sporadic	USA Russia Sweden	[112]
72.37	126.48	Low center polygon, Samoylov Island, Lena Delta	0-50 cm	NA	-6 to 0	Continuous	Russia	[113]
63.3	-142.7	80-yr-old black spruce, E. Tanana River Valley	Organic	21	0	Discontin.	USA	[114]
68.61 68.61 64.88 63.57	-149.20 -149.59 -147.78 -157.73	Tundra and boreal peatlands, Toolik, Fairbanks, Innoko NWR	Active layer, permafrost	30	-4, -0.5	Continuous, Discontin.	USA	[115]
69.99 69.38 69.43 69.15	-148.69 -148.74 -148.70 -148.85	Wet nonacidic tundra, Arctic coastal plain, lowland Moist acidic tundra, Sagwon Hills, lowland Moist acidic tundra, Sagwon Hills, upland Moist acidic tundra, Happy Valley, upland	0-100 cm active layer, permafrost	30	-1, 1	Continuous	USA	U1**

* Sites spanned these coordinates
** Lead providers of unpublished data: U1: Matamala/Jastrow

SI Table 6. Model fit parameters for boosted regression tree 'Spatial' model, in which input variables were derived from geospatial data, compared to 'Site' model, in which input data included both geospatial and *in situ* data.

Model fit parameters	**Spatial**	**Site model**
N	950	1014
# trees	4950	6250
mean total deviance	0.108	0.107
mean residual deviance	0.037	0.029
estimated cv deviance	0.054	0.048
cv deviance se	0.004	0.005
training data correlation	0.813	0.857
cv correlation	0.709	0.746
% deviance explained	49%	55%

SI Table 7. Earth System Models (ESMs) used for the boosted regression tree future scenario model estimates. The 'x' indicates ESM model ensemble combinations used for each predictor.

ESM	GPP	LAI	Precip.	Air temp.	Soil temp.	Soil moist.
ACCESS1-3			x	x	x	x
CanESM2		x	x			x
CCSM4	x	x	x	x		x
CMCC-CM			x	x	x	
CNRM-CM5					x	x
CSIRO-Mk3-6-0			x	x		
GISS-E2-H	x		x	x	x	x
GISS-E2-R	x		x	x	x	x
HadGEM2-CC			x	x		x
HadGEM2-ES			x	x		x
IMNCM4	x	x	x	x	x	x
MIROC5			x	x	x	x
MIROC-ESM				x	x	x
MPI-ESM-LR	x	x	x	x	x	
MPI-ESM-MR	x		x	x		
MRI-ESM1					x	
NorEsm1-M	x	x	x	x	x	x

SI Table 8. Input variables to the boosted regression tree Spatial model (geospatial data) are in bold. Inputs to the alternative Site model, which included geospatial and *in situ* data, are italicized. 'Publication' indicates that the variables were *in situ* data extracted from published and unpublished studies.

Variable	Description	Source
Moisture	Mean surface non-frozen moisture (cm^3 cm^{-3}) for measurement month or, if frozen, last unfrozen period; for pre-2002 data, used 2002-2016 mean	AMSR[8]
Moisture-JJ	Mean surface non-frozen moisture (cm^3 cm^{-3}) in prior June- July; for pre-2002 data, used 2002-2016 mean	AMSR[8]
Landcover	Vegetation/landcover type (SI Table 4); adjusted based on site descriptions	CAVM/CCI[16,17]; publication
Tree Cover	Tree cover (%), measurement year, or 2000 for pre-2000 data	MODIS[19]
Clay	Soil clay content (%) in top 30 cm	SoilGrids[13]
GPP	GPP (g C m^{-2} yr^{-1}) from previous growing season	SMAP L4C NATURE runs[21]
Soil Temp	Average monthly soil temperature (K) in the first soil layer during measurement month	MERRA 2[7]
LAI	Maximum leaf area index (LAI); July 10 - Aug 20	MODIS[20]
Sand	Soil sand content (%) in top 30 cm	SoilGrids[13]
SOC	Soil organic carbon (SOC; %) in top 30 cm	SoilGrids[13]
Air Temp	Average air temp (K) at 2 m height during measurement month	MERRA 2[7]
Landcover	Vegetation/landcover type (SI Table 4); adjusted based on site descriptions; classes grouped if < 3 locations per group	CAVM/CCI[16,17]; publication
EVI	Mean enhanced vegetation index (EVI) for growing season prior to winter flux	MODIS[18]
*GPP**	Gross primary productivity from previous/same year as measurement, *in situ* data	publication
*Method**	Measurement method (See SI text for categories)	publication
PZI	Permafrost zonation index	[15]
*Season**	Early (Oct-Nov), mid (Dec-Feb), late winter (Mar-Apr), or full winter	publication
Moisture-RA	Average monthly soil wetness fraction for surface to root zone from measurement month or last unfrozen period	MERRA 2[7]
*Soil Temp**	Soil temperature for the measurement month, *in situ* data	publication

References

1 Pribyl, D. W. A critical review of the conventional SOC to SOM conversion factor. *Geoderma* **156**, 75–83 (2010).

2 Björkman, M. P., et. al. A comparison of annual and seasonal carbon dioxide effluxes between sub-Arctic Sweden and High-Arctic Svalbard. *Polar Res.* **29**, 75-84 (2010).

3 Goodrich, J. P., et. al. Impact of different eddy covariance sensors, site set-up, and maintenance on the annual balance of CO_2 and CH_4 in the harsh Arctic environment. *Agric. For. Meteorol.* **228-229**, 239-251 (2016).

4 Webb, E. E., et. al. Increased wintertime CO_2 loss as a result of sustained tundra warming. *Biogeosciences* **121**, 1-17 (2016).

5 Goulden, M. L., Wofsy, S. C., Harden, J. W., Trumbore, S. E., Crill, P. M., Gower, S. T., Fries, T., Daube, B. C., Fan, S. M., Sutton, D. J., Bazzaz, A., Munger, J. W. Sensitivity of boreal carbon balance to soil thaw. *Science* **9**, 214-217 (1998).

6 Hijmans, R. J., Cameron, S. E., Parra, J. L., Jones, P. G., & Jarvis, A. Very high resolution interpolated climate surfaces for global land areas. *Int. J. Climatol.* **25**, 1965–1978 (2005).

7 Gelaro, R., et. al. The modern-era retrospective analysis for research and applications, version 2 (MERRA-2). *J. Clim.* **30**, 5419–5454 (2017).

8 Du, J., et al. A global satellite environmental data record derived from AMSR-E and AMSR2 microwave Earth observations. *Earth Syst. Sci. Data* **9**, 791–808 (2017).

9 Reichle, R. H., et al. Assessment of MERRA-2 Land Surface Hydrology Estimates. *J. Clim.* **30**, 2937–2960 (2017).

10 Elberling, B. Annual soil CO_2 effluxes in the High Arctic: The role of snow thickness and vegetation type. *Soil Biol. Biochem.* **39**, 646-654 (2007).

11 Kim, Y. Effect of ablation rings and soil temperature on 3-year spring CO_2 efflux along the Dalton Highway, Alaska. *Biogeosciences* **11**, 6539–6552 (2014).

12 Hugelius, G., et. al. Estimated stocks of circumpolar permafrost carbon with quantified uncertainty ranges and identified data gaps. *Biogeosciences* **11**, 6573–6593 (2014).

13 Hengl, T., et al. SoilGrids250m: Global gridded soil information based on machine learning. *PLoS One* **12**, 1-40 (2017).

14 Brown, J., Ferrians, O., Heginbottom, J., & Melnikov, E. Circum-Arctic map of permafrost and ground-ice conditions, version 2. National Snow and Ice Data Center, Boulder: Colorado, USA. (2002).

15 Gruber, S., The Climate Data Guide: Global Permafrost Zonation Index Map. https://climatedataguide.ucar.edu/climate-data/global-permafrost-zonation-index-map (2013).

16 Walker, D. A., et al. The circumpolar Arctic vegetation map. *J. Veg. Sci.* **16**, 267–282 (2005).

17 ESA Land Cover CCI Product User Guide V2. https://www.esa-landcover-cci.org/ (2014).

18 Didan, K. MYD13A2 MODIS/Aqua Vegetation Indices 16-Day L3 Global 1 km SIN Grid V006. NASA EOSDIS LP DAAC. doi:10.5067/MODIS/MYD13A2.006.

19 DiMiceli, C. M., et al. Annual Global Automated MODIS Vegetation Continuous Fields (MOD44B) at 250 m Spatial Resolution for Data Years Beginning Day 65, 2000 - 2010, Collection 5 Percent Tree Cover., doi:at <www.landcover.org/data/vcf/> (2011).

20 Myneni, R., Knyazikhin, Y., & Park, T. MOD15A2H MODIS Leaf Area Index/FPAR 8-Day L4 Global 500 m SIN Grid V006. NASA EOSDIS Land Processes DAAC. (2015).
21 Jones, L. A., et al. The SMAP level 4 carbon product for monitoring ecosystem land–atmosphere CO_2 Exchange. *IEEE Trans. Geosci. Remote Sens.* **55**, 6517–6532 (2017).
22 Running, S. W., Zhao, M. User's Guide. Daily GPP and Annual NPP (MOD17A2/A3) Products NASA Earth Observing System MODIS Land Algorithm. Version 3.0 for Collection 6 (2015).
23 Carroll, M. L., et al. Development of an operational land water mask for MODIS Collection 6, and influence on downstream data products. *Int. J. Digit. Earth* **10**, 207–218 (2017).
24 Brodzik, M. J., Billingsley, B., Haran, T., Raup, B. & Savoie, M. H. EASE-Grid 2.0: Incremental but significant improvements for Earth-gridded data sets. *ISPRS Int. J. Geo-Information* **1**, 32-45 (2012).
25 Burba, G. G., McDermitt, D. K., Grelle, A., Anderson, D. J., & Xu, L. Addressing the influence of instrument surface heat exchange on the measurements of CO_2 flux from open-path gas analyzers. *Glob. Chang. Biol.* **14**, 1854–1876 (2008).
26 De'ath, G. Boosted trees for ecological modeling and prediction. *Ecology* **88**, 243–251 (2007).
27 R Core Team. R: A language and environment for statistical computing. (2016).
28 Ridgeway, G. Generalized Boosted Models: A guide to the gbm package. 1-12 (2007).
29 Elith, J., Leathwick, J. R. & Hastie, T. A working guide to boosted regression trees. *J. Anim. Ecol.* **77,** 802-813 (2008).
30 McGuire, A. D., et. al. An assessment of the carbon balance of Arctic tundra: Comparisons among observations, process models, and atmospheric inversions. *Biogeosciences* **9**, 3185–3204 (2012).
31 Oleson, K. W., et al. NCAR/TN-503+STR NCAR Technical Note. CLM5 Documentation at <http://www.cesm.ucar.edu/models/cesm2/land/> (2013).
32 CLM Documentation at *<http://www.cesm.ucar.edu/models/cesm2/land/>*.
33 Lawrence, D. M., Koven, C. D., Swenson, S. C., Riley, W. J., & Slater, A. G. Permafrost thaw and resulting soil moisture changes regulate projected high-latitude CO_2 and CH_4 emissions. *Environ. Res. Lett.* **10**, doi:94011 (2015).
34 Zhang, Z., et al. Emerging role of wetland methane emissions in driving 21st century climate change. *Proc. Natl. Acad. Sci.* **114**, doi:201618765 (2017).
35 Sitch, S., et al. Evaluation of ecosystem dynamics, plant geography and terrestrial carbon cycling in the LPJ dynamic global vegetation model. *Glob. Chang. Biol.* **9**, 161–185 (2003).
36 Bloom, A. A., Exbrayat, J.-F., van der Velde, I. R., Feng, L., & Williams, M. The decadal state of the terrestrial carbon cycle: Global retrievals of terrestrial carbon allocation, pools, and residence times. *Proc. Natl. Acad. Sci.* **113**, 1285–1290 (2016).
37 Tramontana, G., et. al. Predicting carbon dioxide and energy fluxes across global FLUXNET sites with regression algorithms. *Biogeosciences* **13**, 4291–4313 (2016).
38 Knutti, R., Masson, D., & Gettelman, A. Climate model genealogy: Generation CMIP5 and how we got there. *Geophys. Res. Lett.* **40**, 1194–1199 (2013).
39 Rogers, B. M. et. al. Impacts of climate change on fire regimes and carbon stocks of the U.S. Pacific Northwest. *J. Geophys. Res. Biogeosciences* **116,** doi:10.1029/2011JG001695

(2011).
40 Leathwick, J. R., Elith, J., Francis, M. P., Hastie, T., & Taylor, P. Variation in demersal fish species richness in the oceans surrounding New Zealand: An analysis using boosted regression trees. *Mar. Ecol. Prog. Ser.* **321**, 267–281 (2006).
41 Winston, G. C., Sundquist, E. T., & Stephens, B. B. Winter CO_2 fluxes in a boreal forest. *J. Geophys. Res. Biogeosciences* **102**, 795–804 (1997).
42 Joiner, D. W., Lafleur, P. M., McCaughey, J. H., & Bartlett, P. A. Interannual variability in carbon dioxide exchanges at a boreal wetland in the BOREAS northern study area. *J. Geophys. Res. Biogeosciences* **104**, 27663–27672 (1999).
43 Ives, S. L., Sullivan, P. F., Dial, R., Berg, E. E., & Welker, J. M. CO_2 exchange along a hydrologic gradient in the Kenai Lowlands, AK: Feedback implications of wetland drying and vegetation succession. *Ecohydrol.* **6**, 38–50 (2013).
44 Arneth, A., et al. Comparative ecosystem–atmosphere exchange of energy and mass in a European Russian and a central Siberian bog II. Interseasonal and interannual variability of CO_2 fluxes. *Tellus B Chem. Phys. Meteorol.* **54**, 514–530 (2002).
45 Arneth, A., Lloyd, J., Shibistova, O., Sogachev, A. & Kolle, O. Spring in the boreal environment: Observations on pre- and post-melt energy and CO_2 fluxes in two central Siberian ecosystems. *Boreal Environ. Res.* **11**, 311–328 (2006).
46 Sullivan, P. F., Welker, J. M., Arens, S. J. T. T., Sveinbjoernsson, B., & Sveinbjörnsson, B. Continuous estimates of CO_2 efflux from arctic and boreal soils during the snow-covered season in Alaska. *J. Geophys. Res. Biogeosciences* 113, doi:10.1029/2008JG000715 (2008).
47 Helbig, M., et al. Direct and indirect climate change effects on carbon dioxide fluxes in a thawing boreal forest–wetland landscape. *Glob. Chang. Biol.* **23**, 3231–3248 (2017).
48 Dolman, A. J., et al. Net ecosystem exchange of carbon dioxide and water of far eastern Siberian Larch (Larix cajanderii) on permafrost. *Biogeosciences* **1**, 133–146 (2004).
49 Belshe, E. F., Schuur, E. A. G., Bolker, B. M., & Bracho, R. Incorporating spatial heterogeneity created by permafrost thaw into a landscape carbon estimate. *J. Geophys. Res. Biogeosciences* **117**, 1–14 (2012).
50 Celis, G., et al. Tundra is a consistent source of CO_2 at a site with progressive permafrost thaw during 6 years of chamber and eddy covariance measurements. *J. Geophys. Res. Biogeosciences* **122**, 1471–1485 (2017).
51 Vogel, J., Schuur, E. A. G., Trucco, C., & Lee, H. Response of CO_2 exchange in a tussock tundra ecosystem to permafrost thaw and thermokarst development. *J. Geophys. Res. Biogeosciences* **114**, doi:10.1029/2008JG000901 (2009).
52 Trucco, C., et al. Seven-year trends of CO_2 exchange in a tundra ecosystem affected by long-term permafrost thaw. *J. Geophys. Res. Biogeosciences* **117,** doi:10.1029/2011JG001907 (2012).
53 Natali, S. M., Schuur, E. A. G., Trucco, C., Hicks Pries, C. E., et al. Effects of experimental warming of air, soil and permafrost on carbon balance in Alaskan tundra. *Glob. Chan. Biol.* **17**, 1394-1407 (2011).
54 Natali, S. M., Schuur, E. A. G. G., Webb, E. E., Pries, C. E. H. H., & Crummer, K. G. Permafrost degradation stimulates carbon loss from experimentally warmed tundra. *Ecology* **95**, 602–608 (2014).

55 Welp, L. R., Randerson, J. T., & Liu, H. P. The sensitivity of carbon fluxes to spring warming and summer drought depends on plant functional type in boreal forest ecosystems. *Agric. For. Meteorol.* **147**, 72–185 (2007).
56 Wickland, K. P., Striegl, R. G., Neff, J. C., & Sachs, T. Effects of permafrost melting on CO_2 and CH_4 exchange of a poorly drained black spruce lowland. *J. Geophys. Res. Biogeosciences* **111**, 1–13 (2006).
57 Euskirchen, E. S., Edgar, C. W., Turetsky, M. R., Waldrop, M. P., & Harden, J. W. Differential response of carbon fluxes to climate in three peatland ecosystems that vary in the presence and stability of permafrost. *J. Geophys. Res. Biogeosciences* **119**, 1576–1595 (2014).
58 Grogan, P., & Chapin, F. S. Arctic soil respiration: Effects of climate and vegetation depend on season. *Ecosystems* **2**, 451–459 (1999).
59 Vogel, J. G., Valentine, D. W., & Ruess, R. W. Soil and root respiration in mature Alaskan black spruce forests that vary in soil organic matter decomposition rates. *Can. J. For. Res.* **35**, 161–174 (2005).
60 Grogan, P. Cold season respiration across a Low Arctic landscape: The influence of vegetation type, snow depth, and interannual climatic variation. *Arctic, Antarct. Alp. Res.* **44**, 446–456 (2012).
61 Nobrega, S., & Grogan, P. Deeper snow enhances winter respiration from both plant-associated and bulk soil carbon pools in birch hummock tundra. *Ecosystems* **10**, 419–431 (2007).
62 Kim, Y., Park, S. J., Lee, B. Y., & Risk, D. Continuous measurement of soil carbon efflux with Forced Diffusion (FD) chambers in a tundra ecosystem of Alaska. *Sci. Total Environ.* **566**, 175–184 (2016).
63 Kim, Y., et al. Assessment of winter fluxes of CO_2 and CH_4 in boreal forest soils of central Alaska estimated by the profile method and the chamber method: A diagnosis of methane emission and implications for the regional carbon budget. *Tellus, Ser. B Chem. Phys. Meteorol.* **59**, 223–233 (2007).
64 Kim, Y., Kodama, Y., & Fochesatto, G. J. Environmental factors regulating winter CO_2 flux in snow-covered black forest soil of Interior Alaska. *Geochemical Journal* **51**, 359-371(2017).
65 Ueyama, M., Iwata, H., & Harazono, Y. Autumn warming reduces the CO_2 sink of a black spruce forest in interior Alaska based on a nine-year eddy covariance measurement. *Glob. Chang. Biol.* **20**, 1161–1173 (2014).
66 Kim, Y., et al. Latitudinal distribution of soil CO_2 efflux and temperature along the Dalton Highway, Alaska. *Polar Sci.* **7**, 162–173 (2013).
67 Heikkinen, J. E. P., Elsakov, V., & Martikainen, P. J. Carbon dioxide and methane dynamics and annual carbon balance in tundra wetland in NE Europe, Russia. *Global Biogeochem. Cycles* 16, https://doi.org/10.1029/2002GB001930 (2002).
68 Sullivan, P. F. Snow distribution, soil temperature and late winter CO_2 efflux from soils near the Arctic treeline in northwest Alaska. *Biogeochemistry* **99**, 65–77 (2010).
69 Kim, Y., et al. Constraint of soil moisture on CO_2 efflux from tundra lichen, moss, and tussock in Council, Alaska, using a hierarchical Bayesian model. *Biogeosciences* **11**, 5567–5579 (2014).
70 Aurela, M., et al. Carbon dioxide exchange on a northern boreal fen. *Boreal Environ. Res.* **14**, 699–710 (2009).

71 Larsen, K. S., Ibrom, A., Grogan, P., Jonasson, S., Michelsen, A., & Beier, C. Significance of cold-season respiration and photosynthesis in a subarctic heath ecosystem in Northern Sweden. *Glob. Chang. Biol.*, **13,** 1498-1508 **(**2007).
72 Grogan, P., & Jonasson, S. Ecosystem CO_2 production during winter in a Swedish subarctic region: the relative importance of climate and vegetation type. *Glob. Chang. Biol.* **12**, 1479–1495 (2006).
73 Björkman, M. P. et. al. Temporal patterns of CO_2, CH_4 and N_2O fluxes and soil microbial structure within snow-covered Alpine plant communities. *Glob. Biogeochem. Cy.* 24, doi:10.1029/2009GB003667 (2007).
74 Larsen, K. S., Grogan, P., Jonasson, S., & Michelsen, A. Respiration and microbial dynamics in two subarctic ecosystems during winter and spring thaw: Effects of increased snow depth. *Arctic, Antarct. Alp. Res.* **39**, 268-276 (2007).
75 Grogan, P., & Jonasson, S. Temperature and substrate controls on intra-annual variation in ecosystem respiration in two subarctic vegetation types. *Glob. Chang. Biol.* **11**, 465–475 (2005).
76 Grogan, P., Illeris, L., Michelsen, A., & Jonasson, S. Respiration of recently-fixed plant carbon dominates mid-winter ecosystem CO_2 production in sub-arctic heath tundra. *Clim. Change* **50**, 129–142 (2001).
77 Olefeldt, D., et al. Net carbon accumulation of a high-latitude permafrost palsa mire similar to permafrost-free peatlands. *Geophys. Res. Lett.* **39** doi:10.1029/2011GL050355 (2012).
78 Kade, A., Bret-Harte, M. S., Euskirchen, E. S. E. S., Edgar, C., & Fulweber, R. A. . Upscaling of CO_2 fluxes from heterogeneous tundra plant communities in Arctic Alaska. *J. Geophys. Res. Biogeosciences* **117**, 1-11 (2012).
79 Euskirchen, E. S., Bret-Harte, M. S., Shaver, G. R., Edgar, C. W., Romanovsky, V. E. . Long-term release of carbon dioxide from arctic tundra ecosystems in Alaska. *Ecosystems* **20**, 960–974 (2017).
80 Euskirchen, E. S., Bret-Harte, M. S., Scott, G. J., Edgar, C., & Shaver, G. R. Seasonal patterns of carbon dioxide and water fluxes in three representative tundra ecosystems in northern Alaska. *Ecosphere* **3**, 1-19 (2012).
81 Corradi, C., Kolle, O., Walter, K., Zimov, S. A., & Schulze, E. D. Carbon dioxide and methane exchange of a north-east Siberian tussock tundra. *Glob. Chang. Biol.* **11**, 1910–1925 (2005).
82 Welker, J. M., Fahnestock, J. T., Jones, M. H. Annual CO_2 flux in dry and moist arctic tundra: field responses to increases in summer temperatures and winter snow depth. *Clim. Change* **44**, 139-150 (2000).
83 Fahnestock, J. T., Jones, M. H., Brooks, P. D., Walker, D. A., & Welker, J. M. Winter and early spring CO_2 efflux from tundra communities of northern Alaska. *J. Geophys. Res. Atmos.* **103**, 29023–29027 (1998).
84 Oechel, W. C., Vourlitis, G., & Hastings, S. J. Cold season CO_2 emission from arctic soils. *Global Biogeochem. Cycles* **11**, 163–172 (1997).
85 Zimov, S. A. Winter biotic activity and production of CO_2 in Siberian soils: a factor in the greenhouse effect. *J. Geophys. Res. Atmos.* **98**, 5017–5023 (1993).
86 Zimov, S. A., et al. Siberian CO_2 efflux in winter as a CO_2 source and cause of seasonality in atmospheric CO_2. *Clim. Change* **33**, 111–120 (1996).

87 Fedorov-Davydov, D. G. Respiration activity in tundra biocenoses and soils of the Kolyma Lowland. *Eurasian Soil Sci.* **31**, 263–273 (1998).
88 Schimel, J. P., Bilbrough, C., & Welker, J. M. Increased snow depth affects microbial activity and nitrogen mineralization in two Arctic tundra communities. *Soil Biol. Biochem.* **36**, 217–227 (2004).
89 Aurela, M., Laurila, T., & Tuovinen, J. P. Annual CO_2 balance of a subarctic fen in northern Europe: Importance of the wintertime efflux. *J. Geophys. Res. Atmos.* **107**, 1–12 (2002).
90 Aurela, M., Laurila, T., & Tuovinen, J. P. The timing of snow melt controls the annual CO_2 balance in a subarctic fen. *Geophys. Res. Lett.* **31**, 3–6 (2004).
91 Oechel, W. C., et al. A scaling approach for quantifying the net CO_2 flux of the Kuparuk River Basin, Alaska. *Glob. Chang. Biol.* **6**, 160–173 (2000).
92 Jones, M. H., Fahnesstock, J. T., & Welker, J. M. Early and late winter CO_2 efflux from Arctic tundra in the Kuparuk River watershed, Alaska. *Arctic, Antarct. Alp. Res.* **31**, 187–190 (1999).
93 Oechel, W. C., et al. Acclimation of ecosystem CO_2 exchange in the Alaskan Arctic in response to decadal climate warming. *Nature* **406**, 978–981 (2000).
94 Oechel, W. C., Laskowski, C. A., Burba, G., Gioli, B., & Kalhori, A. A. M. Annual patterns and budget of CO_2 flux in an Arctic tussock tundra ecosystem. *J. Geophys. Res. Biogeosciences* **119**, 323–339 (2014).
95 Christiansen, C. T., Schmidt, N. M. & Michelsen, A. High Arctic dry heath CO_2 exchange during the early cold season. *Ecosystems* **15**, 1083-1092 (2012).
96 Christiansen, C. T., Svendsen, S. H., Schmidt, N. M., & Michelsen, A. High arctic heath soil respiration and biogeochemical dynamics during summer and autumn freeze-in – effects of long-term enhanced water and nutrient supply. *Glob. Chang. Biol.* **18**, 3224–3236 (2012).
97 Nordstroem, C., Soegaard, H., Christensen, T. R., Friborg, T., & Hansen, B. U. Seasonal carbon dioxide balance and respiration of a high-arctic fen ecosystem in NE-Greenland. *Theor. Appl. Climatol.* **70**, 149–166 (2001).
98 Pirk, N., et al. Snowpack fluxes of methane and carbon dioxide from high Arctic tundra. *J. Geophys. Res. Biogeosciences* **121**, 2886–2900 (2016).
99 Rogers, M. C., Sullivan, P. F., Welker, J. M. Evidence of nonlinearity in the response of net ecosystem CO_2 exchange to increasing levels of winter snow depth in the high Arctic of Northwestern Greenland. *Arct. Antarc. Alpine Res.* **43**, 95-106 (2011).
100 Strebel, D., Elberling, B., Morgner, E., Knicker, H. E., & Cooper, E. J. Cold-season soil respiration in response to grazing and warming in High-Arctic Svalbard. *Polar Res.* **29**, 46–57 (2010).
101 Morgner, E., Elberling, B., Strebel, D., & Cooper, E. J. The importance of winter in annual ecosystem respiration in the High Arctic: Effects of snow depth in two vegetation types. *Polar Res.* **29**, 58–74 (2010).
102 Semenchuk, P. R., Christiansen, C. T., Grogan, P., Elberling, B., & Cooper, E. J. Long-term experimentally deepened snow decreases growing-season respiration in a low- and high-arctic tundra ecosystem. *J. Geophys. Res. Biogeosciences* **121**, 1236–1248 (2016).
103 Sjögersten, S., van der Wal, R., & Woodin, S. J. Habitat type determines herbivory controls over CO_2 fluxes in a warmer Arctic. *Ecology* **89**, 2103–2116 (2008).

104 Pirk, N., et al. Spatial variability of CO_2 uptake in polygonal tundra: assessing low-frequency disturbances in eddy covariance flux estimates. *Biogeosciences* **14**, 3157–3169 (2017).
105 Welker, J. M., Fahnestock, J. T., Henry, G. H. R., O'Dea, K. W., & Chimner, R. A. CO_2 exchange in three Canadian High Arctic ecosystems: Response to long-term experimental warming. *Glob. Chang. Biol.* **10**, 1981–1995 (2004).
106 Luërs, J., et al. Annual CO_2 budget and seasonal CO_2 exchange signals at a high Arctic permafrost site on Spitsbergen, Svalbard archipelago. *Biogeosciences* **11**, 6307–6322 (2014).
107 Oquist, M. G., et al. Water availability controls microbial temperature responses in frozen soil CO2 production. *Glob. Chang. Biol.* **15**, 2715–2722 (2009).
108 Larsen, K. S., Jonasson, S., & Michelsen, A. Repeated freeze-thaw cycles and their effects on biological processes in two arctic ecosystem types. *Appl. Soil Ecol.* **21**, 187–195 (2002).
109 Michaelson, G. J., Ping, C.L. Soil organic carbon and CO_2 respiration at subzero temperature in soils of Arctic Alaska. *J.G.R. Atmos.* **108** (2003).
110 Elberling, B., Brandt, K.K. Uncoupling of microbial CO_2 production and release in frozen soil and its implications for field studies of arctic C cycling. *Soil Biol. Biogeochem.* **35**, 263-272 (2003).
111 Mikan, C. J., Schimel, J. P., & Doyle, A. P. Temperature controls of microbial respiration in arctic tundra soils above and below freezing. *Soil Biol. Biochem.* **34**, 1785–1795 (2002).
112 Panikov, N. S., Flanagan, P. W., Oechel, W. C., Mastepanov, M. A., & Christensen, T. R. Microbial activity in soils frozen to below -39°C. *Soil Biol. Biochem.* **38**, 785–794 (2006).
113 Müller-Lupp, W., & Bölter, M. Effect of soil freezing on physical and microbiological properties of permafrost-affected soils. *Permafrost* 801–805 (2003).
114 O'Neill, K. P., Richter, D. D., & Kasischke, E. S. Succession-driven changes in soil respiration following fire in black spruce stands of interior Alaska. *Biogeochemistry* **80**, 1-20 (2006).
115 Treat, C. C., et al. Temperature and peat type control CO_2 and CH_4 production in Alaskan permafrost peats. *Glob. Chang. Biol.* **20**, 2674–2686 (2014).